Electronic Supplementary Information

Naphthaldehyde-based Schiff Base Dyes: Aggregation-induced Emission and High-contrast Reversible Mechanochromic Luminescence

Lingyi Shen,‡[a] Chang-Jin Yu,‡[a] Hai-Fang Xie,[a] Na Xu,[a] Hong Xu,[a] Ya-Li Huang,[a] Carl Redshaw,*[b] Xing Feng*[c] and Qi-Long Zhang*[a]

[a] *Research Center for Molecular Medical Engineering, School of Basic Medical Science, Guizhou Medical University, Guiyang 550004, China. gzuqlzhang@126.com*

[b] *Department of Chemistry, University of Hull, Cottingham Road, Hull, Yorkshire HU6 7RX, UK. c.redshaw@hull.ac.uk*

[c] *Guangdong Provincial Key Laboratory of Functional Soft Condensed Matter, School of Material and Energy, Guangdong University of Technology, Guangzhou 510006, P. R. China. hyxhn@sina.com*

‡ *These authors contributed equally to this work.*

Table and Contents

Experimental Section·····S1 **3**

Fig. S1 ^{1}H NMR spectrum of probe HNP **3**

Fig. S2 ^{13}C NMR spectrum of probe HNP **4**

Fig. S3 HR ESI-MS spectrum of probe HNP **4**

Fig. S4 Absorption (Abs.) and fluorescence (PL) spectra of HNP in different solution **5**

Fig. S5 UV-vis absorption of the probe at different water content in THF. **5**

Fig. S6 Fluorescence (PL) spectra of HNP at different water content **5**

Fig. S7 Absorption (Abs.) and fluorescence (PL) spectra of HNP in different pH. **6**

Fig. S8 The solid UV-vis absorption spectra of HNP-y and when ground and fuming. **6**

Fig. S9 ORTEP diagram of HNP-r HNP-y and HNP-r **7**

Fig. S10 The XRD patterns of HNP-y and HNP-r powders, and the simulated XRD patterns of HNP-y and HNP-r crystals. **7**

Fig. S11 Bar diagram of the competitive experiments of various metal **8**

Fig. S12 UV-visible absorption spectra and fluorescence emission spectra of different concentrations of Cu^{2+} on HNP **9**

Fig. S13 Job's plot of HNP and Cu^{2+} in THF solution **9**

Fig. S14 Linear fitting of the emission data upon addition of Cu^{2+} **10**

Fig. S15 The Benesi–Hildebrand plot of $1/(F-F_0)$ *versus* $1/[Cu^{2+}]$ **11**

Fig. S16 ORTEP diagram of HNP-Cu and 1D columnar structure of HNP-Cu **11**

Table S1 Crystallographic data and refinement details **12**

Supplementary References……S2 **12**

S1. Experimental section

Synthesis of HNP: *N*,*N*'-(2-aminophenyl)-2,6-dicarboxylimide pyridine (0.347 g, 1 mmol) which was synthesized according to the literature method was dissolved in 50 mL methanol and 2-hydroxy-1-naphthaldehyde (0.350 g, 2 mmol) was added. After stirring for 10 minutes, 10 µL H_2SO_4 was drip added to the resulting mixture. Stirring was continued for 8 h at room temperature to afford a red precipitate. The resulting red precipitate was collected by filtration to give the compound **HNP**. (0.510 g, 78%). On the other hand, 60 µL H_2SO_4 was drip added to the reaction mixture, following given a yellow product. ^{1}H NMR (400 MHz, $CDCl_3$-TMS, 298 K):δ/ppm 16.03 (s, 1H, naphthyl-O*H*), 16.02 (s, 1H, naphthyl-O*H*), 10.60 (s, 2H, N*H*), 8.61 (s, 1H, C*H*=N), 8.59 (s, 1H, C*H*=N), 8.33 (d, *J*= 8.0 Hz, 2H, Py-*H*), 8.30 (d, *J*= 4.0 Hz, 2H, naphthyl-*H*), 8.19 (t, *J*= 8.0 Hz, 1H, Py-*H*), 7.61 (d, *J*= 7.6 Hz, 2H, Ph-*H*), 7.42 (t, *J*= 7.6 Hz, 2H, Ph-*H*), 7.34 (m, 2H, naphthyl-*H*), 7.29 (d, 4H, *J*= 4.0 Hz naphthyl-*H*), 7.25 (d, 2H, *J*= 8.0 Hz, naphthyl-*H*), 7.17 (t, *J*= 8.0 Hz, 2H, Ph-*H*), 6.85 (d, 2H, *J*= 4.0 Hz naphthyl-*H*), 6.17 (d, 2H, *J*= 8.0 Hz, Ph-*H*). ESI-MS m/z: calcd. for $[C_{41}H_{29}N_5O_4+H]^+$, 656.2292; found, 656.2291. M.p.: 274−275°C.

Synthesis of HNP-Cu: $CuCl_2$ (0.135 g, 1 mmol) was added to a stirred solution of **HNP** (0.328 g, 0.5 mmol) in methanol (60 mL), and the mixture was stirred for 2 h. The resulting brown precipitate was collected by filtration. The filtrate was recrystallized from methanol. X-ray quality brown single crystals of **HNP-Cu** were obtained by slow evaporation of a saturated methanol solution.

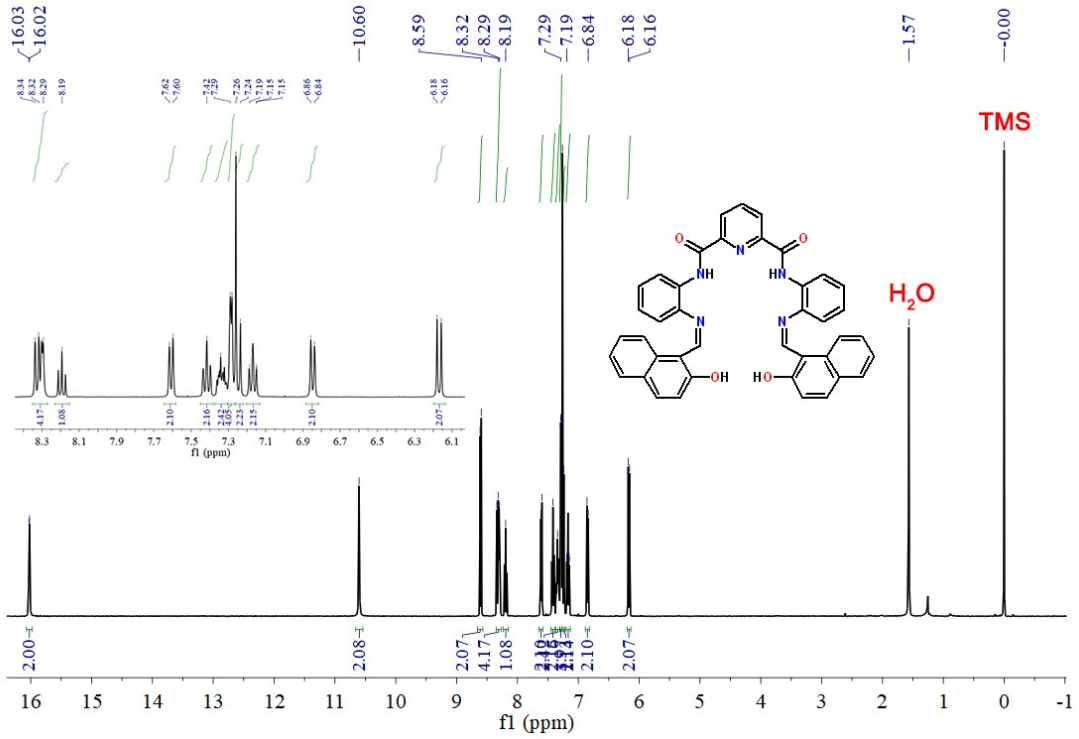

Fig. S1 ^{1}H NMR (400 MHz, $CDCl_3$, 298 K) of probe **HNP**.

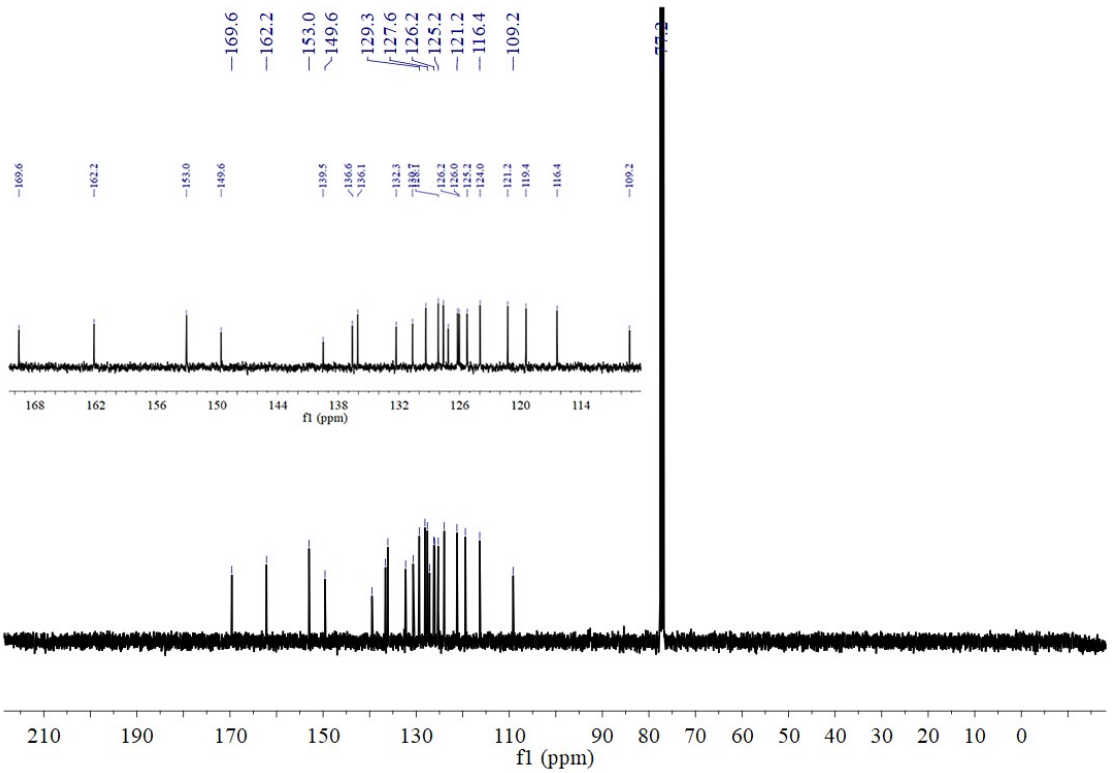

Fig. S2 ^{13}C NMR (400 MHz, $CDCl_3$, 298 K) of probe **HNP**.

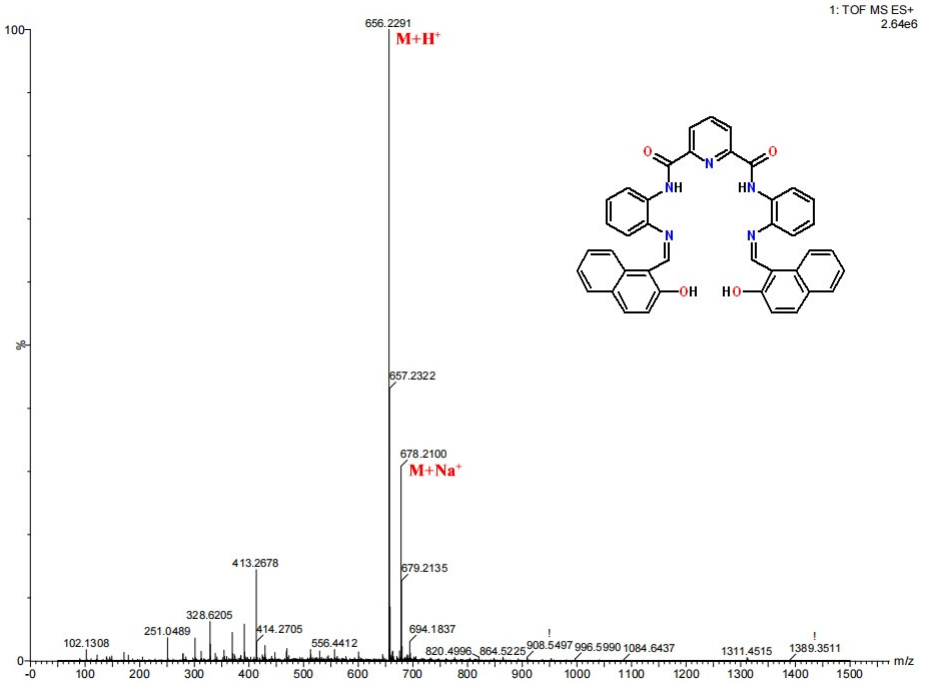

Fig. S3 HR ESI-MS spectrum of probe **HNP.**

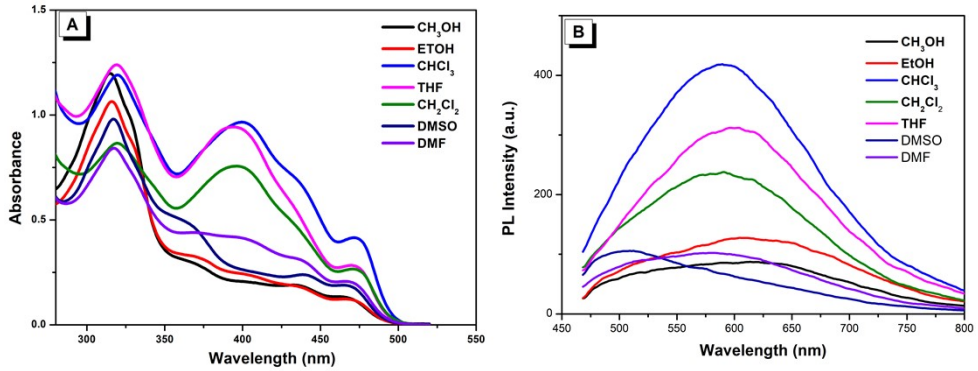

Fig. S4 Absorption (Abs.) and fluorescence (PL) spectra of **HNP** in different solvents.

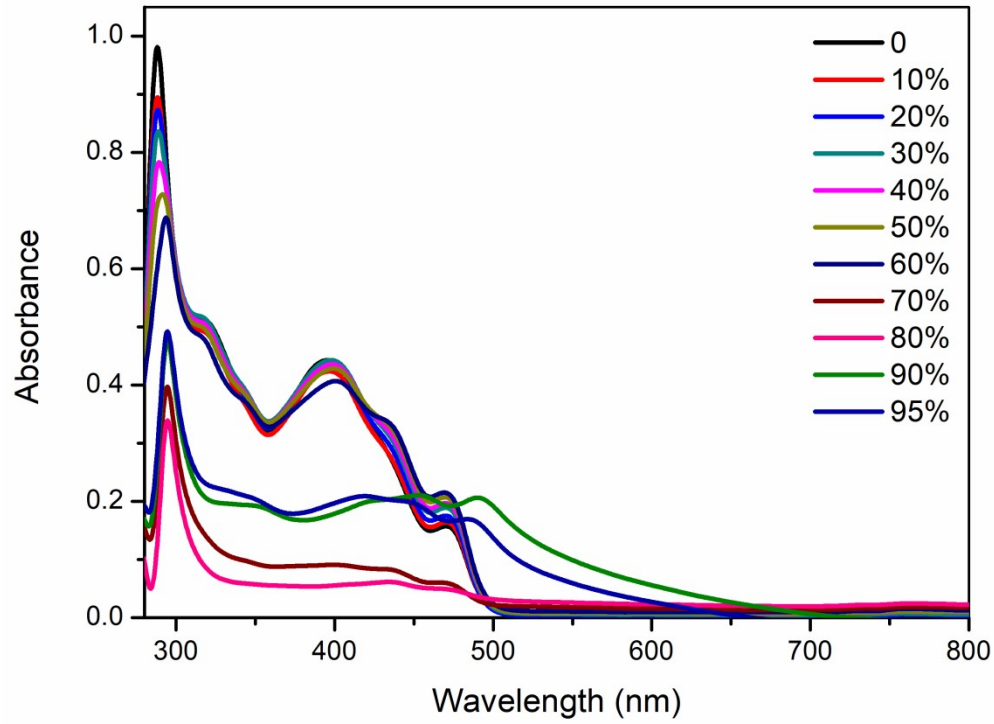

Fig. S5 UV-vis absorption of the probe (2.00×10^{-5} mol/L) at different water content in THF.

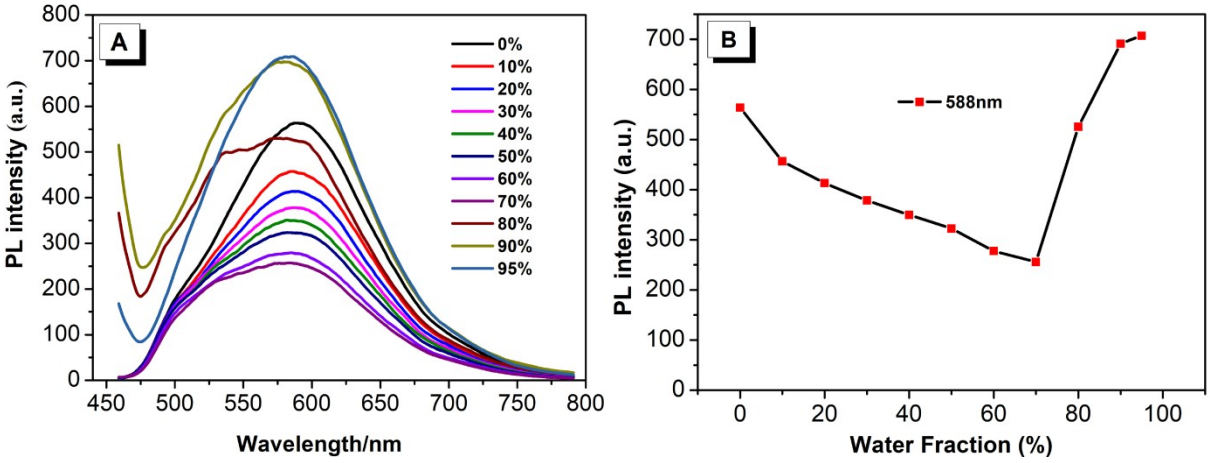

Fig. S6 (a) Fluorescence spectra of the fluorescent probe (5.00×10^{-5} mol/L) at different water content (λ_{ex} = 440 nm) in THF. (b) Effect of water volume fraction on fluorescence probe at 588 nm.

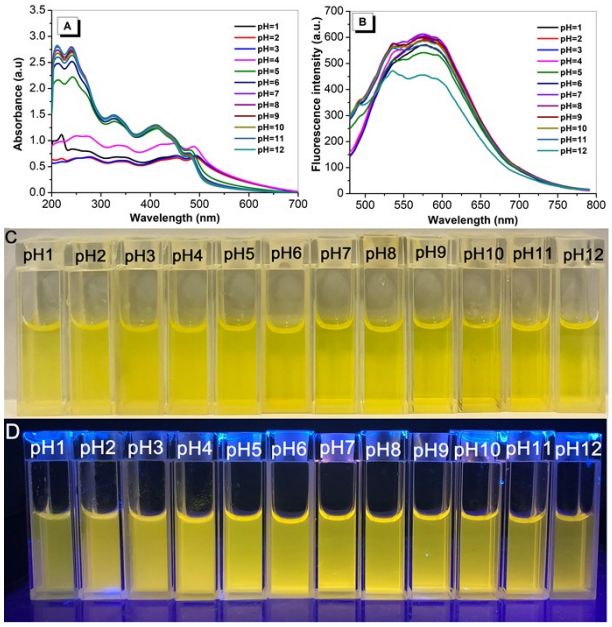

Fig. S7 Absorption (Abs.) and fluorescence (PL) spectra of **HNP** (5.00×10^{-5} mol/L, V_{THF}/V_{water} = 1/9, Tris-HCL buffer) in different pH.

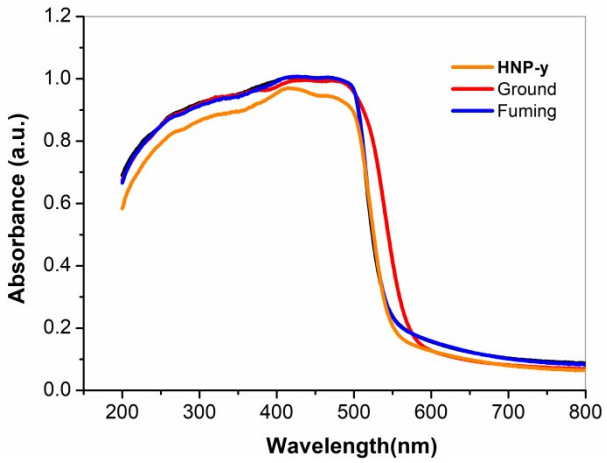

Fig. S8 UV-vis solid absorption spectra of **HNP-y** and when ground and fuming.

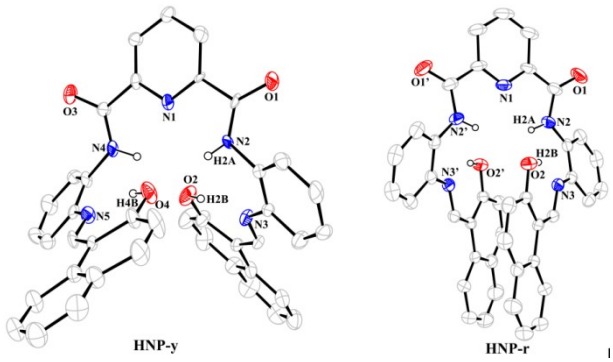

Fig. S9 ORTEP diagram of **HNP-y** and **HNP-r** (Thermal ellipsoids are set at the 30% probability level and some hydrogen atoms and solvent molecules were omitted for clarity).

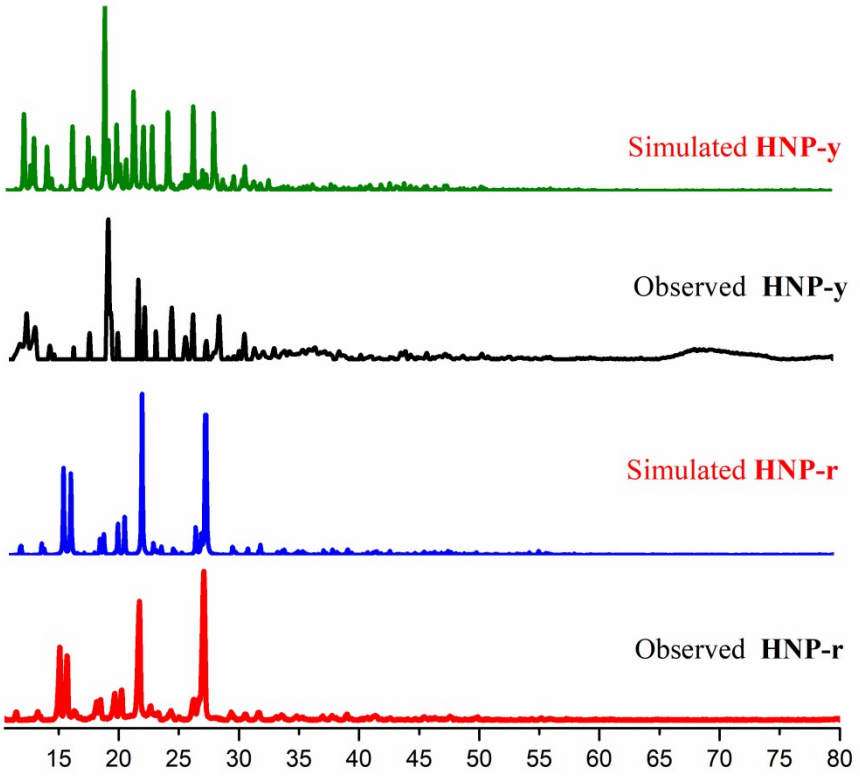

Fig. S10 The XRD patterns of **HNP-y** and **HNP-r** powders, and the simulated XRD patterns of **HNP-y** and **HNP-r** crystals.

Interaction time between fluorescent probe and Cu^{2+}

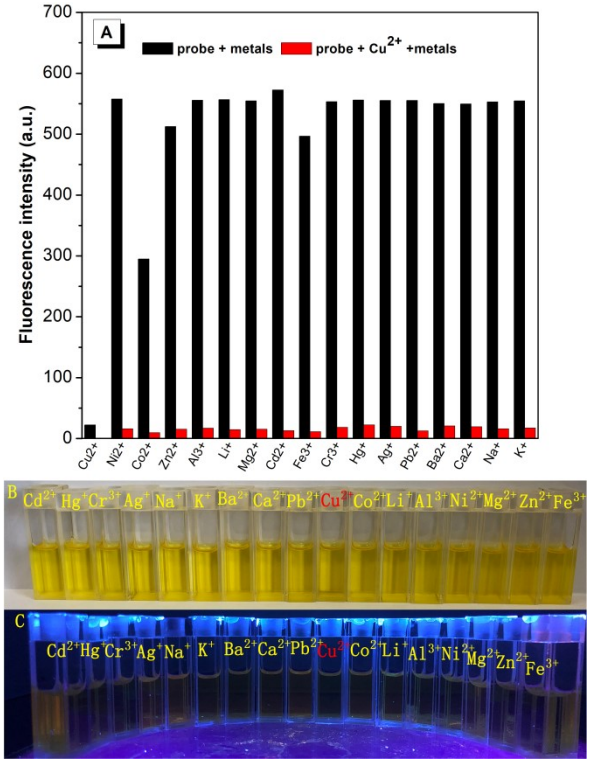

Fig. S11 Bar diagram of the competitive experiments of various metal. ($\lambda_{ex}/\lambda_{em}$ = 440 nm/588 nm).

Under the same conditions, fluorescence titration experiments with Cu^{2+} were carried out. Experimental process: In THF solution, the fixed probe concentration was 5.00×10^{-5} mol/L, and different concentrations of Cu^{2+} were added respectively. After shaking, the UV-visible absorption spectrum and fluorescence spectrum were recorded. Results: As shown in Fig. S12, in THF solution, the absorbance of the probe at 396 nm gradually decreased with the increase of Cu^{2+} concentration, meanwhile, a new absorbance at 443 nm gradually increased. Moreover, the fluorescence intensity of the probe decreased gradually at 588 nm, and the fluorescence quenching rate reached 95.35% when two equivalents Cu^{2+} were added. Based on the UV titration experiments and the fluorescence titration experiments, the ratio between the probe and Cu^{2+} is 1:2.

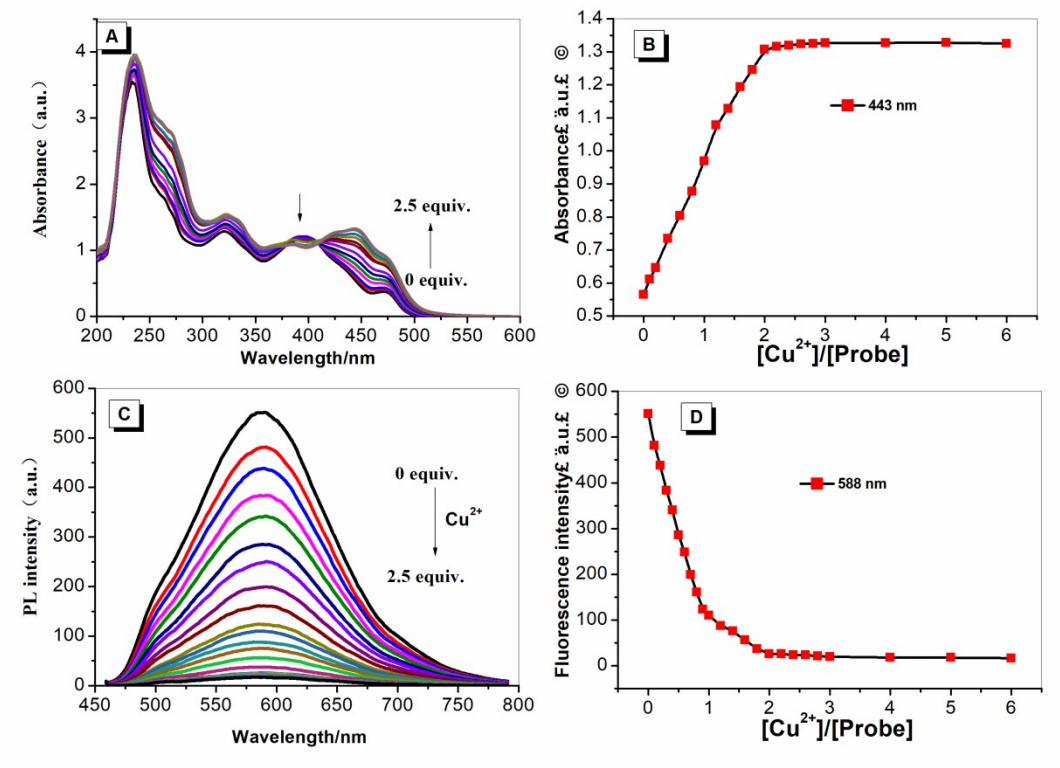

Fig. S12 UV-visible absorption spectra of different concentrations of Cu^{2+} on fluorescence probe; (B) UV-visible line diagram of $N_{Cu^{2+}}/N$probe system at 443nm; (C) Fluorescence spectra of different concentrations of Cu^{2+} on fluorescence probes; (D) fluorescence line chart of $N_{Cu^{2+}}/N$probe system at 588nm.

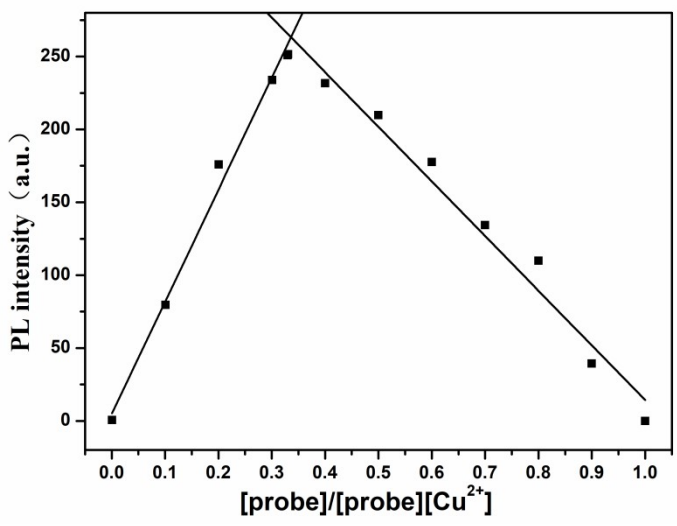

Fig. S13 Job's plot for the determination of the stoichiometry of **HNP** and Cu^{2+} in THF solution, the total concentration of **L** and Cu^{2+} was 100 μM.

Determination of detection limits

The detection limit of probe **HNP** for Cu^{2+} can also be obtained through the fluorescence titration experiments of Cu^{2+}. Under the same conditions, 10 groups of blank experiments were carried out first, that is, only probe (5.0×10^{-6} mol/L) was added without Cu^{2+}, and the fluorescence value at wavelength 588 nm was calculated as 0.55. Then 10 points in Cu^{2+} fluorescence titration experiments where the fluorescence decreased with the increase of Cu^{2+} concentration were taken, and the calibration curve of fluorescence intensity change of probe with Cu^{2+} concentration was made. The fluorescence intensity of the system was linearly correlated with the concentration of Cu^{2+} over the range 5.0×10^{-6} mol/L to 4.5×10^{-5} mol/L, with a correlation coefficient R^2=0.99487 (n=10). The linear equation y= Ax +b can be obtained from Fig. S14, where a=-9.39289×10^{6}, b=532.44855; then according to the formula: detection limit = 3SD/S, S is the slope, that is A, so it can be concluded that the detection limit is 1.8×10^{-7} mol/L.

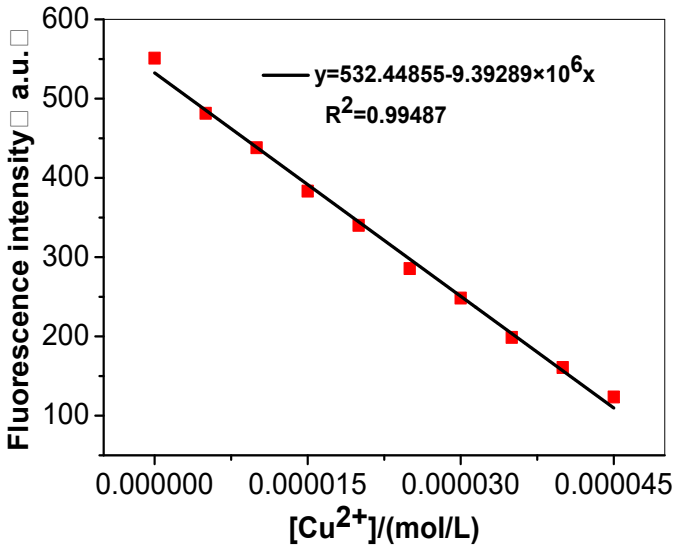

Fig. S14 Linear fitting of the emission data upon addition of Cu^{2+}.

Determination of binding constants

The binding constant K_a was calculated from the experimental results of the fluorescence titrations. In the fluorescence titration experiments for Cu^{2+}, the fluorescence decreased with the increase of Cu^{2+} concentration at 4-10 points, and then according to the Benesi-Hildebrand equation $F\text{-}F_0 = \triangle F = [Cu^{2+}](F_{max}\text{-}F_0)/(1/K_a + [Cu^{2+}])$, we can calculate the binding constant Ka between the probe and Cu^{2+}, where F represents the fluorescence intensity at wavelength 588nm with a specific Cu^{2+} concentration, F_0 represents the fluorescence intensity at wavelength 588 nm without Cu^{2+} addition, and Fmax represents the minimum fluorescence intensity at wavelength 588 nm in the Cu^{2+} titration experiments. As shown in Fig. S15, a linear graph was made with $1/[Cu^{2+}]$ as abscissa and $1/(F\text{-}F_0)$ as ordinate, and the linear equation y= Ax +b was obtained, and then combined with the Benesi-Hildebrand equation, and the final binding constant is $Ka = B/A = -4.76003\times10^{-4}/-8.35374\times10^{-8} = 5.6980\times10^{3}$ mol/L.

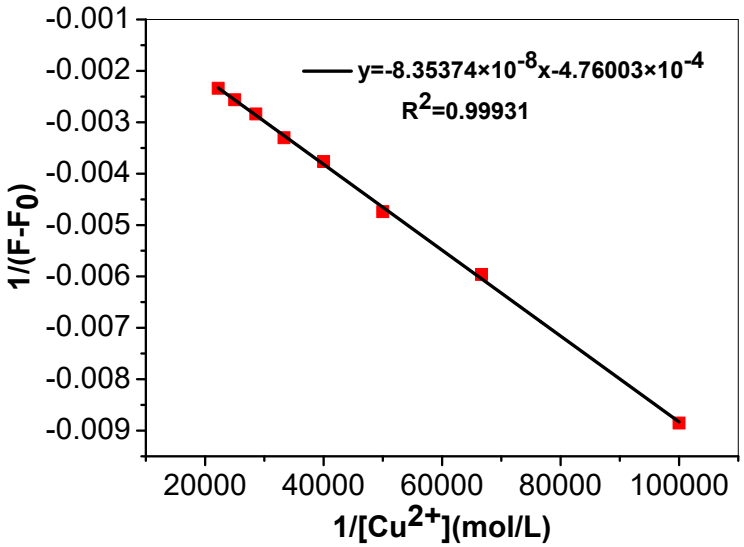

Fig. S15 The Benesi–Hildebrand plot of $1/(F-F_0)$ *versus* $1/[Cu^{2+}]$.

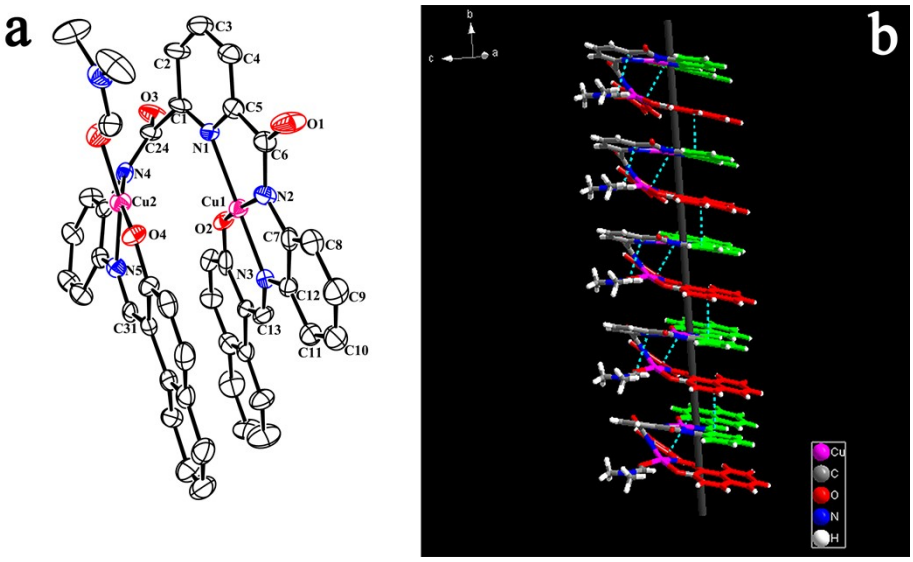

Fig. S16 (a) ORTEP diagram of **HNP-Cu.** (Thermal ellipsoids are set at the 30% probability level and all hydrogen atoms and solvent molecules were omitted for clarity). **(b)** 1D columnar structure of **HNP-Cu**. The blue dotted lines indicate the intermolecular π···π interactions and intramolecular hydrogen bond interactions.

X-ray crystal structure determination. X-ray diffraction data for compounds **HNP-y, HNP-r** and **HNP-Cu** were collected on a Bruker SMART APEX II diffractometer at room temperature (297 K) with graphite-monochromated Mo Kα radiation (λ = 0.71073 Å). An empirical absorption correction using SADABS was applied for all data.[2] The structures were solved and refined to convergence on F^2 for all independent reflections by the full-matrix least squares method using the SHELXL−2014 programs[3] and OLEX2 1.2.[4]
CCDC: 2174338, **HNP-y**; 2174339, **HNP-r** and 2174340, **HNP-Cu:** contain the supplementary crystallographic data for this paper. These data can be obtained free of charge from the Cambridge Crystallographic Data Centre www.ccdc.cam.ac.uk/data_request/cif

Table S1. Crystallographic data and refinement details for **HNP-y**, **HNP-r** and **HNP-Cu**.

Parameter	HNP-y	HNP-r	HNP-Cu
CCDC Number	2174338	2174339	2174340
Formula	$C_{41}H_{29}N_5O_4$	$C_{41}H_{29}N_5O_4$	$C_{44}H_{32}Cu_2N_6O_5$
Formula weight	655.69	655.69	851.83
Crystal system, space group	Triclinic *P*-1	Monoclinic *C2/c*	Orthorhombic $Pna2_1$
a /Å	8.865(4)	18.257(3)	24.656(6)
b /Å	12.406(5)	15.436(3)	7.0427(15)
c /Å	14.817(6)	13.494(3)	42.311(10)
α /deg	84.607(18)	90	90
β /deg	86.15(2)	122.871(4)	90
γ /deg	86.94(2)	90	90
V /Å^3	1616.8(12)	3194.0(11)	7347(3)
Z	2	4	8
D_{calcd} /g cm^{-3}	1.347	1.364	1.540
F(000)	684.0	1368.0	3488.0
μ /mm^{-1}	0.089	0.090	1.216
2*ϑ* range	5.226–49.998	5.278–49.996	5.074–49.998
Independent reflections	5675	12239	12126
R_{int}	0.2172	0.1124	0.0935
Final R_1, wR_2 values *(I> 2σ(I))*	0.1785, 0.3989	0.0629, 0.1169	0.0625, 0.1572
R_1, wR_2 (all data)	0.3157, 0.4497	0.1507, 0.1409	0.1061, 0.1794
GOF (F^2)	1.244	0.937	1.026

S2. Supplemental References

1. H.-F. Xie, C.-J.Yu, Y.-L.Huang, H. Xu, Q.-L. Zhang, X.-H. Sun, X. Feng, C. Redshaw, A turn-off fluorescent probe for the detection of Cu $^{2+}$ based on a tetraphenylethylene-functionalized salicylaldehyde Schiff-base. *Mater. Chem. Front*., 2020, **4**, 1500-1506.
2. G. M. Sheldrick, Program SADABS: Area-Detector Absorption Correction, University of Göttingen, Germany. 1996.
3. G. M. Sheldrick, *Acta Crystallogr., Sect. C: Cryst. Struct. Commun*. 2015, **71**, 3-8.
4. O. V. Dolomanov, L. J. Bourhis, R. J. Gildea, J. A. K. Howard and H. *J.* Puschmann, *Appl. Cryst.,* 2009, **42**, 339-341.